Fabrication and Characterization of Multiferroics

Prateek Gupta

A dissertation submitted for the partial fulfilment of BS-MS dual degree in Science

Indian Institute of Science Education and Research Mohali

April 2014

Certificate of Examination

This is to certify that the dissertation titled **"Fabrication and Characterization of Multiferroics"** submitted by **Prateek Gupta** (Reg. No. MS09096) for the partial fulfillment of BS-MS dual degree programme of the Institute, has been examined by the thesis committee duly appointed by the Institute. The committee finds the work done by the candidate satisfactory and recommends that the report be accepted.

Dr. Sanjeev Kumar Dr. Yogesh Singh Dr. Goutam Sheet
(Supervisor)

Dated: April 25, 2014

Declaration

The work presented in this dissertation has been carried out by me under the guidance of Dr. Goutam Sheet at the Indian Institute of Science Education and Research Mohali.

This work has not been submitted in part or in full for a degree, a diploma, or a fellowship to any other university or institute. Whenever contributions of others are involved, every effort is made to indicate this clearly, with due acknowledgement of collaborative research and discussions. This thesis is a bonafide record of original work done by me and all sources listed within have been detailed in the bibliography.

Prateek Gupta
(Candidate)

Dated: April 25, 2014

In my capacity as the supervisor of the candidate's project work, I certify that the above statements by the candidate are true to the best of my knowledge.

Dr. Goutam Sheet
(Supervisor)

Acknowledgement

I would like to express my gratitude to my supervisor Dr Goutam Sheet, Condensed Matter Group, Department of Physics, IISER Mohali, for guiding me through this project. I am thankful to Dr Yogesh Singh and Dr Sanjeev Kumar for helping me out and giving me suggestions. I thank IISER Mohali for providing me financial support through INSPIRE fellowship.

I am thankful to Ashima Arora, Jithin B.P., Avtar Singh, Jagmeet Sekhon and Leena Aggarwal (my lab members) for supporting me throughout my time at lab. They have been very friendly and helping and made life at lab fun.

Finally I would to thank my family and friends for their understanding, encouragement and love.

List of Figures

Abstract

Magnetoelectric multiferroics are materials which exhibit co-existing magnetic and ferroelectric phases, with coupling between magnetic and electric ordering. These have become a very hot area of research in the past decade or so; mainly due to their novel physical properties and applications in data storage devices, sensors and spintronics. The project investigates the multiferroic properties of double perovskite Y_2NiMnO_6 in bulk as well as polycrystalline thin films.

Y_2NiMnO_6 has been shown theoretically to be polar in its magnetic ground state with an intrinsic polarization comparable with other magnetically-driven ferroelectrics like $TbMnO_3$, $TbMn_2O_5$, $HoMnO_3$.[1]. To investigate these properties the bulk sample was prepared by using solid state synthesis and thin film of the material were deposited on different substrates using pulsed laser deposition method. Characterization of material was done by x-ray diffraction, atomic force microscopy and piezoresponse force microscopy.

Contents

Chapter 1

Introduction

1.1 Background

Complex oxides show a wide range of physical properties, including ferromagnetism, ferroelectricity, superconductivity, strongly correlated electron behavior and magnetoresistance, which have interested scientific community for decades. Materials which exhibit magnetic and ferroelectric properties have been extensively studied bacause of their applications in memory devices and sensors.Because of the size dependence of physical and chemical properties, novel applications of these materials are expected in nanoscale forms.

Ferromagnetic materials show spontaneous magnetization and the alignment of spins can be changed by an external magnetic field. Similarly, ferroelectric materials exhibit spontaneous polarization which can be switched by an external electric field. A number of similarities exist between ferromagnetism and ferroelectricity like anomalies at critical temperature, domain structures and hysteresis behaviour. These similarities are very significant considering the origin of ferromagnetism and ferroelectricity is different in solid oxides: whereas magnetism arises from ordering of electron spins in incomplete ionic shells, ferroelectricity is due to an asymmetric charge distribution due to the off-center shifts of negative and positive ions.

Multiferroics are materials that exhibit more that one ferroic order simultaneously. Ferromagnetism, ferroelectricity, ferroelasticity and ferrotoroidicity are four basic primary ferroic orders. A small class of materials exhibit coupling between ferromagnetism and ferroelectricity and are called magneto-electric multiferroics. In these select materials, electric field can not only reorient polarization but also change the spin directions, or magnetic field can control magnetization as well as induce ferroelectricity. New devices can be made using this property of magneto-electric multiferroics.

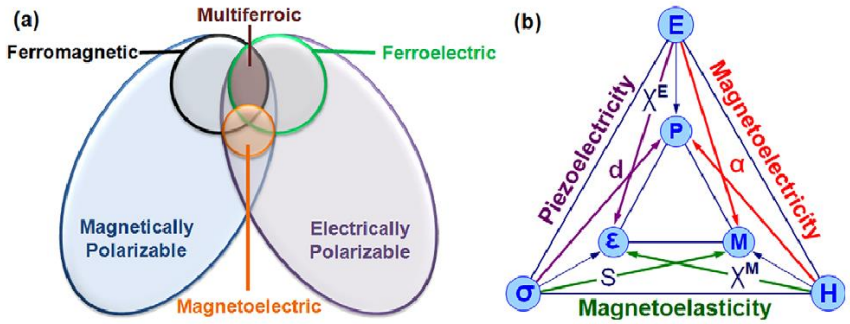

Figure 1.1: (a) Relationship between multiferroic and magnetoelectric materials (b) Schematic representation of different types of coupling present in materials [9]

Materials that show multiferroicity are very scarce (Figure 1.1) as multiferroicity is determined by a number of factors, including crystal structure symmetry, electronic properties, and chemical properties. Infact, there are only thirteen point groups that can give rise to multiferroicity [15]. Moreover, there are only a few magneto-electric multiferroics due to mutual exclusivity of origins of magnetism and electric polarization (ferromagnetism needs transition metals with unpaired *3d* electrons and unfilled *3d* orbitals, whereas ferroelectric polarization needs transition metals with filled *3d* orbitals).

1.2 Double Perovskite Multiferroics

Double perovskite compounds, $A_2BB'O_6$, present a unique opportunity to induce and control multiferroic behaviour in oxides. As discussed in the previous section that magnetism and ferroelectricity have mutually exclusive mechanisms, double perovskite compounds provide a system in which a strong coupling between them can be achieved. Recently, double perovskite compounds have been theoretically predicted to be multiferroics [1][16][17]. The polarization in this system can be induced by 1) structural distortion arising from different chemical valencies of ions occupying B and B' sites or 2) ferroelectric ions occupying the A sites. There are some reports on the magnetic and ferroelectric properties of double perovskite compounds; including La_2CoMnO_6, Bi_2FeMnO_6, Bi_2NiMnO_6, and Bi_2FeCrO_6.

1.3 Multiferroic Composite Systems

Previously discussed double perovskite multiferroics lie in the category of single phase multiferroics. Other types of single phase multiferroics are $REMnO_3(RE: Y, Ho - Lu), BiFeO_3$ type, $REMn_2O_5(RE: La, Pr, Nd, Sm - Eu)$ and fluoride multifer-

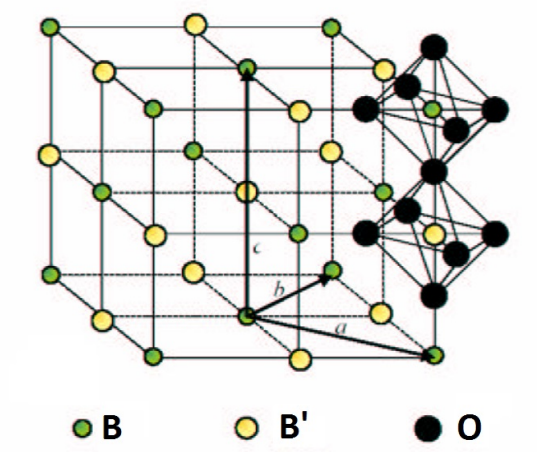

Figure 1.2: Double perovskite structure.

roics. In the known single phase multiferroics, the magneto-electric coupling is very weak and ordering temperature is very less than room temperature for applications. However, in multiferroic composites the magneto-electric coupling is very high above room temperature and they are ready for technological applications. Ferroelectric and ferromagnetic materials can be mixed together and magnetoelectric coupling can be achieved to form a multiferroic. The interface of an epitaxial film of a ferromagnet like $La_{1-x}Sr_xMnO_3$ grown on a ferroelectric substrate having a similar crystal structure like $SrTiO_3$ can be an example of a composite multiferroic.

For particulate composites that are also piezoelectric, there can be many connectivity schemes. Among composite systems, particulate ceramic composites are most easily prepared by the conventional sintering technique. Powders of piezoelectric ceramics and magnetic oxides are mixed and pellets are formed followed by a sintering process.

1.4 Applications

1.4.1 Magnetic Field Sensors

Magneto-electric multiferroics can be used to detect magnetic fields. The magnetic phase in a magneto-electric multiferroics responds to an external magnetic field and induces a proportional change in the charge distribution in the ferroelectric phase. This small change in charge density can be detected by a current detector. Highly sensitive magnetic field sensors can be made from multiferroics having a high magneto-electric coupling. The multiferroic multilayer configuration of these devices enables ultra low frequency detection of magnetic field variations. These sensors are of ultra high sensitivity and detect magnetic fields as low as 10^{-12} T.

1.4.2 Memory Devices

The most desirable applications of multiferroics is in case of memory devices. Multiferroic materials that can be integrated with semiconductors are of great interest. Devices like high density ferroelectric memory (FeRAM), ferroelectric field effect transistors (FeFET-RAM) and the concept of four-state memories can revolutionize the field of computation.

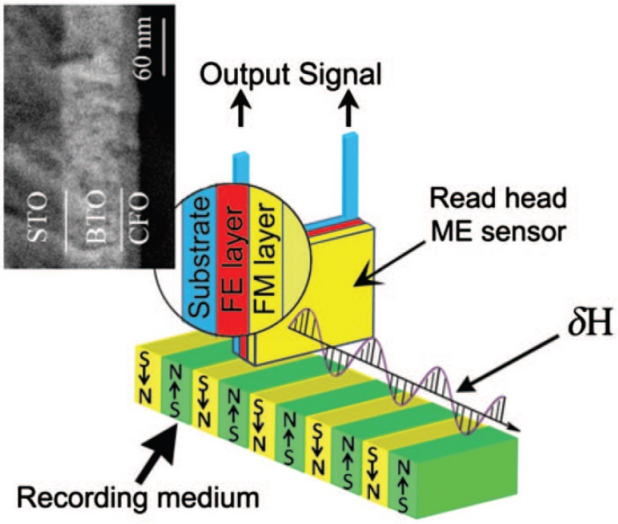

Figure 1.3: Schematic of a read head sensor based on bi-layered heterostructures [18].

For memory applications, the main route is integration with semiconductors. Ferroelectric thin films can be deposited on metallic electrodes and on semiconductors forming a non-volatile memory structure. Using the fact that magneto-electric multiferroics have both magnetic and ferroelectric properties, concept of four state memory has been proposed based on depositing thin films of multiferroic on a single crystal oxide substrate [19].

Many multiferroic materials have been proposed suitable for realization of high density FeRAMs of which $BiFeO_3$ and $YMnO_3$ look promising for they do not interact with semiconductor substrates because of their low dielectric constants.

In this thesis, the second and third chapter provide theoretical understanding of the physics behind multiferroics and the basic principles of the experimental techniques used in this work. The last chapter includes the experimental work on synthesis and characterization of properties of multiferroic systems.

Chapter 2

Ferromagnetism and Ferroelectricity

2.1 Ferromagnetism

The characteristic feature of a ferromagnet is it's spontaneous magnetization, which is result of the alignment of atomic magnetic moments within the material. The magnetic moment of an atom originates from the electron's spin and it's motion around the nucleus. The coupling between electron's spin and its orbital motion around the nucleus is described by the spin orbit hamiltonian defined as follows:

$$\hat{H}_{SO} = \frac{1}{2m_e c^2}\frac{1}{r}(\frac{\partial V}{\partial r})\hat{L}\cdot\hat{S} \tag{2.1}$$

Electrons having the same quantum state can not align their spins parallel. The Pauli exclusion principle prevents them from doing so and thus a spin imbalance arises in electron shells that are not full. In a many electron system, coulomb force repels the electrons which are in close proximity to minimize the coulomb energy. Electrons therefore occupy different quantum states first with parallel spins. This gives an atom with incomplete filled shells, a net magnetic moment. Atoms with completely filled electron shells do not have magnetism. In 3d transition metals like Ni, Fe, and Co, the magnetism arises primarily due to the imbalance between the two spin states.

The spontaneous magnetization of ferromagnetic materials happens due to the long range ordering of atomic magnetic moments. Assuming that the electrons are localized, the ordering of magnetic moments is described by Heisenberg hamiltonian defined as:

$$\hat{H} = -\Sigma J_{ij}\mathbf{S_i}\cdot\mathbf{S_j} \tag{2.2}$$

where J_{ij} is the exchange integral and $\mathbf{S_i}, \mathbf{S_j}$ are localized atomic spins. In ferro-

magnetic materials $J_{ij} > 0$ therefore neighbour spins align parallel. This ordering of atomic spins due to exchange interaction happens only upto an ordering temperature, T_c, known as Curie temperature. Beyond this temperature the ferromagnetic ordering is overcome by thermal fluctuations.

The overall behaviour of magnetization in a ferromagnetic material is a consequence of the competition between magnetostatic energy, exchange energy and anisotropy energy. Among these, exchange energy dominates the short range ordering but long range ordering is determined by magnetostatic and anisotropy energies.

2.1.1 Exchange Energy

Exchange energy is a short range interaction and dominates the alignment of atomic spins at short length scales. In ferromagnetic materials, the spins align parallel due to exchange interaction. The direct exchange between two atomic spins is given by the Heisenberg hamiltonian as defined in equation 2.2. The exchange interaction results in an exchange energy density which can be defined as:

$$E_{ex} = A(\nabla \mathbf{m})^2 \tag{2.3}$$

where $\mathbf{m} = \mathbf{M}/M_s$ is the magnetization unit vector and A is the exchange stiffness constant.

2.1.2 Magnetostatic Energy

Magnetostatic (dipole-dipole) forces are long ranged but weak forces. In a uniformly magnetized material, stray magnetic field is created outside the sample and a demagnetizing field is created inside the magnetic material. The magnitude of the magnetostatic energy is significantly smaller than the exchange energy but it operates over longer length scales. The magnetic dipole strength can be written as:

$$\sigma = \mathbf{M} \cdot \mathbf{n} \tag{2.4}$$

where $\mathbf{n}$ is unit vector normal to the interface. The magnetostatic energy density due to stray magnetic fields at the interface can be written as:

$$E_{ms} = -(\frac{\mu_0}{2})\mathbf{H}_d \cdot \mathbf{M} \tag{2.5}$$

where $\mathbf{H}_d$ is the magnetic dipole field created by the magnetization. The demagnetizing field is a consequence of this which anti-aligns with the magnetization inside the

magnetic material. For a material of an arbitrary shape, demagnetizing field is given by:

$$H_d = -NM \tag{2.6}$$

where N is the demagnetizing tensor which is equal to unity for thin films with perpendicular magnetization.

2.1.3 Magnetic Anisotropy Energy

Magnetic anisotropy describes the angular dependence of magnetic energy. In an anisotropic magnetic system, the easy axis is defined as the magnetization orientation with minimum magnetic anisotropy energy and similarly the hard axis is the one aligned with maximum magnetic anisotropic energy. The anisotropy constant K_i is a measure of anisotropic strength and is defined as the energy density associated with an anisotropic contribution, i. In multiferroic systems, the anisotropic energy is dominated by the magnetocrystalline and magnetoelastic contributions.

Magnetocrystalline Anisotropy

Magnetocrystalline anisotropy arises from the symmetry of crystalline lattices and the elongated charge distribution around atoms due to the spin-orbit coupling. If we expand the free energy of a cubic magnetocrystalline system, E_c in terms of directional cosines, m_1, m_2, and m_3, where $m_i = M_i/M_s$, we get

$$E_c = K_1(m_1^2m_2^2 + m_1^2m_3^2 + m_2^2m_3^2) + K_2(m_1^2m_2^2m_3^2)... \tag{2.7}$$

where K_1 and K_2 are first and second order anisotropy constants. In crude terms, the sign of K_1 determines whether $\langle 001 \rangle$ or $\langle 111 \rangle$ are the magnetocrystalline easy axes.

Amorphous ferromagnetic materials exhibit no magnetocrystalline anisotropy since no crystal symmetry is present. Completely randomly oriented polycrystalline materials will exhibit very little magnetocrystalline anisotropy as the magnetocrystalline anisotropy of small regions will cancel over macroscopic length scales.

Magnetoelastic Anisotropy

Magnetoelastic anisotropy arises in the material when a mechanical strain is applied to it. This is also known as inverse magnetostriction effect. The strength of the

magnetoelastic anisotropy is proportional to the stress σ and magnetostriction λ_s of the material. The magnetoelastic anisotropy constant K_{me}, for isotropic materials can be written as

$$K_{me} = -\frac{3\sigma\lambda_s}{2}, \tag{2.8}$$

where σ is proportional to the strain ϵ via Young's modulus Y. Isotropic systems include amorphous films and polycrystalline films with random texture. Magnetoelastic anisotropy in amorphous systems originates from so-called bond-orientation anisotropy, where the anisotropy depends on average bond lengths. The anisotropy of an isotropic system experiencing a uniaxial strain can be written as

$$E_{me} = -K_{me} sin^2\phi \tag{2.9}$$

where ϕ is the angle between the magnetization and the strain axis. The magnetoelastic easy asis can either be parallel or perpendicular to the direction of uniaxial strain. The sign of magnetostriction λ_s and the sign of strain ϵ determine the sign of K_{me}. For example, if a film experiences uniaxial tensile strain ($\epsilon > 0$) and has positive magnetostriction then $K_{me} < 0$ which leads to a minimum E_{me} lying parallel to the direction of the tensile strain axis. If the same film were to experience a compressive strain ($\epsilon < 0$) the magnetoelastic easy axis would lie perpendicular to the strain axis.

For crystalline systems, the magnetoelastic anisotropy depends on the direction of strain with respect to the crystalline axes of the material. The general form of magnetoelastic anisotropy energy in a crystalline system can be written as

$$E_{me} = B_1(\alpha_1^2\epsilon_x + \alpha_2^2\epsilon_y + \alpha_3^2\epsilon_z) + B_2(\alpha_1\alpha_2\epsilon_{xy} + \alpha_2\alpha_3\epsilon_{yz} + \alpha_1\alpha_3\epsilon_{xz}) \tag{2.10}$$

where B_i are the magnetoelastic anisotropy constants, α_i are the directional cosines of the magnetization with respect to the crystalline axes, ϵ_i are normal strains along the crystalline axes and ϵ_{ij} are shear strains.

In epitaxial systems, the magnetocrystalline anisotropy and the magnetoelastic anisotropy both contribute to the total anisotropy energy. For a crystalline material experiencing normal strain the magnetoelastic anisotropy dominates the magnetocrystalline anisotorpy above a critical strain value, ϵ_c which can be written as

$$\epsilon_c = \frac{|K_1|}{|B_1|}. \tag{2.11}$$

2.1.4 Zeeman Energy

The Zeeman energy describes how the magnetization of a magnetic sample interacts with an applied magnetic field. The Zeeman energy can be written as

$$E_z = -\mu_0 \int \mathbf{M} \cdot \mathbf{H} dV, \tag{2.12}$$

where $\mathbf{H}$ is the external field and $\mathbf{M}$ is the magnetization of the sample. For uniform magnetization and uniform external magnetic field, this can be written as an energy density

$$E_z = -\mu_0 M_s H cos(\phi - \theta), \tag{2.13}$$

where $(\phi - \theta)$ is the angle between $\mathbf{M}$ and $\mathbf{H}$ and M_s is the saturation magnetization of the sample.

2.1.5 Magnetic Domains and Domain Walls

Magnetic domains are areas of uniform magnetization separated by magnetic domain walls. These are formed due to competition between short range exchange energy and long range magnetostatic energy. The exchange length is defined as the length below which inter-atomic exchange interactions dominate and can be written as

$$l_{ex} = (A/\mu_0 M_s^2)^{1/2} \tag{2.14}$$

where A is the exchange stiffness and M_s is the saturation magnetization. Magnetic domain formation becomes energetically favorable when the size of a magnetic structure becomes larger than l_{ex}.

If a magnetic sample is placed in an external magnetic field ($\mathbf{H}$), the Zeeman energy E_z will force the magnetization to align with $\mathbf{H}$ above the saturation field. This creates a mono domain state where the magnetization is uniform over the entire sample. The total energy of magnetic domains can be written as the sum of different energy contributions

$$E_{domain} = E_{ex} + E_{ms} + E_c + E_{me} + E_z. \tag{2.15}$$

The domains are formed in a magnetic material as a consequence of minimizing the total energy (E_{domain}) of the magnetic system.
The width of the domain walls (δ_w) that separates magnetic domains is determined by the competition between exchange energy and the magnetic anisotropy energy. Large exchange stiffness widens the domain walls as it minimizes the magnetization rota-

tion between neighboring atomic spins. On the other hand, large magnetic anisotropy decreases the width of the domain wall in order to minimize the energy penalty for having the magnetization pointing away from the magnetic easy axis inside the domain wall.

2.2 Ferroelectricity

Polar materials possess an effective electric dipole moment in the absence of an external electric field. In general, the individual dipoles are randomly oriented in space. In so-called pyroelectric materials, all dipoles are oriented in the same sense, creating a surface charge, which is a measure of spontaneous polarization P_s. Ferroelectrics are a special case of polar materials where spontaneous polarization P_s possess at least two equilibrium states; the direction of the spontaneous polarization vector can be switched between those orientations by an electric field. The crystal symmetry requires that all ferroelectric materials must be pyroelectric and all pyroelectric materials must be piezoelectric. Today, the majority of piezoelectric materials in practical use, with an important exception of quartz, are ferroelectrics.

Most ferroelectric materials undergo a structural phase transition from a high-temperature nonferroelectric (or paraelectric) phase into a low-temperature ferroelectric phase. Some ferroelectrics like $BaTiO_3$, undergo several phase transitions into successive ferroelectric phases. The transition into a ferroelectric phase usually leads to strong anomalies in the dielectric, elastic, thermal and other properties of the material, and is accompanied by changes in the dimensions of the crystal unit cell. The associated strain is called spontaneous strain, x_s. It represents the relative difference in the dimensions of the ferroelectric and paraelectric unit cells.

2.2.1 Ferroelectric Domains

Ferroelectric domains form to minimize the electrostatic energy of the depolarizing fields and the elastic energy associated with the mechanical constraints to which the ferroelectric material is subjected to as it is cooled through the paraelectric-ferroelectric phase transition. Onset of spontaneous polarization at the transition temperature leads to the formation of surface charges. This surface charge produces an electric field, called the depolarizing field E_d, which is oriented oppositely to P_s as shown in Figure 2.1. The depolarizing field will form whenever there is a non homogeneous distribution of spontaneous polarization.

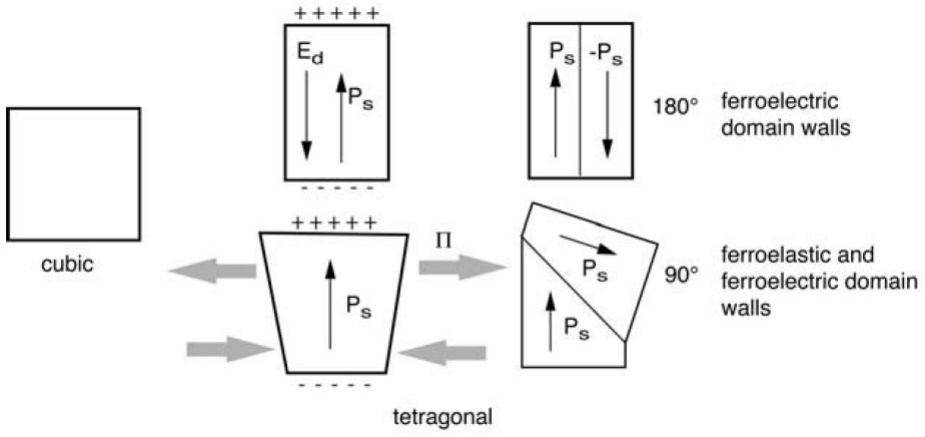

Figure 2.1: Illustration of the formation of 180° and 90° ferroelectric domain walls in a tetragonal perovskite ferroelectric. Tetragonal distortion is exaggerated. Effects of the depolarizing field, E_d and stresses, Π are minimized by creation of domain walls [3].

The electrostatic energy associated with the depolarizing field may be minimized if: (i) the ferroelectric splits into domains with oppositely oriented polarization, Figure 2.1 , or (ii) the depolarizing charge is compensated by electrical conduction through the crystal or by charges from the surrounding material. The depolarizing field often cannot be completely compensated, and as grown ferroelectric crystals often exhibit reduced or even zero pyroelectric and piezoelectric effects due to the presence of ferroelectric domains.

Splitting of a ferroelectric crystal into domains may also occur due to the influence of mechanical stresses, as shown in Figure 2.1. As an example consider a $PbTiO_3$ crystal. Assume that a part of crystal is mechanically compressed along the [100] cubic direction as it is cooled through the phase transition temperature. To minimize the elastic energy, the long c_T axis of the tetragonal cell will develop perpendicularly to the stress. In the unstressed part of the crystal, the polarization may remain parallel to the direction of the stress. The domain walls in $PbTiO_3$ may therefore separate the regions in which polarization orientation is anti-parallel 180° or perpendicular 90° to each other. Both 180° and 90° walls may reduce the effects of the depolarizing electric fields but only formation of 90° walls may minimize the elastic energy. A combination of electrical and elastic boundary conditions to which a crystal is subjected as it is cooled through the ferroelectric phase transition temperature usually leads to a complex domain structure with many 90° and 180° domain walls. Since domain walls themselves carry energy, the resulting domain-wall configuration will be such that the sum of the domain-wall energy, crystal surface energy, and elastic and electric fields energy is minimum.

The domain walls that differ in orientation from the spontaneous polarization vector are called ferroelectric domain walls and those that differ in orientation from the spontaneous strain tensor are called ferroelastic domain walls.

Chapter 3

Experimental Techniques

3.1 Pulsed Laser Deposition

In the pulsed laser deposition method, thin films are prepared by the ablation of one or more targets illuminated by a focussed pulsed-laser beam. This technique was first used by Smith and Turner in 1965 for the preparation of semiconductors and dielectric thin films. Pulsed laser deposition is a very versatile technique. Since the energy source is kept outside the chamber, the use of ultrahigh vacuum and ambient gas atmosphere is possible. Combined with stoichiometry transfer between target and the substrate, it is possible to deposit all kinds of different materials, e.g., high temperature superconductors, oxides, nitrides, carbides, semiconductors, metals and even polymers can be grown with high deposition rates. The pulsed nature of PLD process allows preparation of complex polymer-metal compounds and multilayers. In UHV, implantation and intermixing effects originating in the deposition of energetic particles lead to the formation of metastable phases. The preparation of the films in an inert gas atmosphere makes it even possible to tune the properties of the thin film (stress, reflectivity, texture, magnetic properties,...) by varying the kinetic energy of the deposited particles. All these characteristics make PLD a technique for the growth of high-quality thin films.

3.1.1 Typical Experimental Setups

A typical setup of PLD is shown schematically in Figure 3.1. In an ultra high vacuum (UHV) chamber, elementary or alloy targets are struck at an angle, by a pulsed and focused laser beam. The atoms and ions ablated from the target(s) are deposited on the substrate mounted in front of the target. The substrates are generally mounted with their surface parallel to the surface of the target, with a typical target to substrate being 2-10 cm.

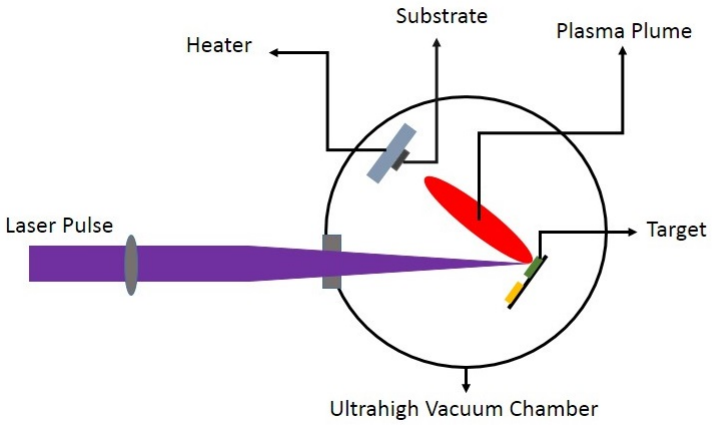

Figure 3.1: Schematic diagram of a Pulsed Laser Deposition setup.

3.1.2 Versatility of PLD

During pulsed laser deposition, many experimental parameters can be controlled, which then have a strong effect on the film properties. First, the laser parameters like fluence, pulse duration and repetition rate can be altered. Second, the preparation conditions, including substrate temperature, target to substance distance, gas environment and pressure, may be varied which all influence the film growth.

UHV and Different Gas Atmospheres

The PLD technique allows preparation of all kinds of oxides, nitrides, but also polymers, or metallic systems. In order to prepare all these different kind of materials, one has to work through ultrahigh vacuum (UHV) or reactive gas atmosphere during deposition. This is possible with PLD since the energy source is located outside the deposition chamber. While growing oxides, the use of oxygen is inevitable in order to achieve sufficient amount of oxygen in the growing oxide film. For instance, for the formation of perovskite structures at high substrate temperatures, an oxygen pressure of about 0.3 mbar is necessary. Also, for many other oxides or nitrides, the necessity of working in a reactive environment makes it difficult for these materials to be prepared by other techniques.

Small Target Size

The PLD technique is also flexible in terms of small size of the target. Since the laser spot is very small, the target area may even be less than $1cm^2$. This allows to

prepare complex samples with enrichments of isotopes or isotropic markers within the deposited film. Being able to prepare samples easily, and in less quantity is especially important if the sample of any component is extremely expensive or impossible to prepare with other techniques. The flexibility of PLD technique also comes in handy due to the possibility of easily exchanging and adjusting the targets.

Stoichiometry Transfer

During PLD, the stoichiometry of the deposited film is very close to that of the used target and therefore, it is possible to prepare stoichiometric thin films using a single alloy bulk target. This so-called "stoichiometry transfer" has made PLD an efficient technique for the growth of complex systems, for instance piezoelectric and ferroelectric materials with perovskite structure.

Stoichiometry transfer between target and substrate is difficult to obtain using other techniques, like, evaporation or magnetron sputtering, by using a single target. This is because partial vapour pressures and sputtering yields of the components are different from each other which gives rise to a different stoichiometry of the thin film growing on a substrate. In case of PLD, in most cases, stoichiometry of the target is is passed on to the film which can be explained as follows.

The fast and strong heating of the target surface by the intense laser beam (typically to temperatures of more than 5000 K within a few ns) ensures that all target components evaporate at the same time, irrespective of their partial binding energies. When the ablation rate is sufficiently high, a so-called Knudsen layer is formed and further heated forming a high temperature plasma, which then expands adiabatically in the direction perpendicular to the surface of the target. Therefore, during PLD, the material transfer between target and substrate occurs in a material package, where the separation of the elements is small. The expansion of the whole package can be described by a shifted Maxwell-Boltzmann center of mass velocity distribution

$$f(v_z) \propto v_z^3 \cdot exp[-m_A(v_z - v_{cm})^2/2kT_{eff}] \tag{3.1}$$

with a center of mass velocity v_{cm} and an effective temperature T_{eff}. Then, adiabatic collision-less expansion occurs transferring the concentration of the plasma plume towards the substrate surface.

Thus, complex structures such as oxides or perovskites are formed again at the substrate surface, when the substrate temperature is high enough, because all com-

ponents are transferred from the target to the substrate at right composition.

3.2 Atomic Force Microscopy

Atomic Force Microscopy is an imaging technique that uses a physical probe to image the topography and the properties a sample. It has a greater advantage over Scanning Tunneling Microscope that it can also probe the properties of non-conducting samples. Since its introduction in 1986 by Gerd Binning, Calvin F. Quate and Christopher Herber, AFM has driven considerable attention in the past few years especially for its atomic resolution of non-conducting samples.

3.2.1 Basic Principle

An elastic cantilever with a tip of dimensions of few nanometers interacts with the sample. A piezo tube on the cantilever is responsible for maintaining the z-distance between the tip and the sample. A feedback loop ensures that the tip does not crashes on the sample while scanning. This feedback loop runs on the basis of a certain feedback parameter (which is different in different scanning modes) which is altered due to interactions between the tip and the sample while scanning. A laser spot falls on top of the cantilever and reflects to the photodiode. Any perturbation in the feedback parameter is detected using a laser and a segmented photodiode. A schematic diagram of AFM assembly is shown in Figure 3.2.

3.2.2 Imaging Modes

Non-Contact Mode

The feedback parameter while scanning in the non-contact mode is the amplitude of oscillations of the tip. The tip is driven by a piezostack at the end of the cantilever at its natural resonant frequency for maximum sensitivity. As the ti-sample distance is reduced, this amplitude of oscillation is damped due to interactions between the tip and the sample. In order to maintain this amplitude at a constant value, the z-piezo contracts or retracts the tip according to the topography of the sample. The voltage supplied to the piezo to move up and down is recorded with the x-y position of the sample. This data provides information about the topographic height of the sample in x-y-z.

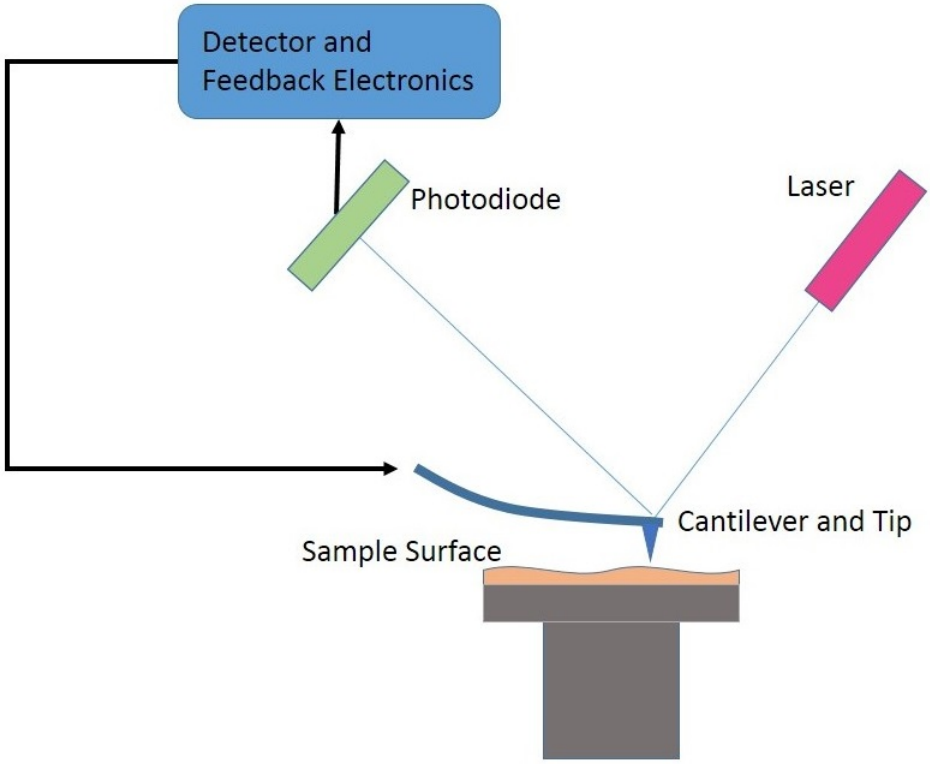

Figure 3.2: Schematic diagram of basic Atomic Force Microscope assembly.

Contact Mode

The tip touches the sample in this mode of imaging i.e. the force between the tip and the sample is repulsive in nature. The cantilever does not oscillates. The feedback parameter the in contact mode is deflection of the tip. Vertical Deflection is defined as difference between the voltage generated in the upper two quadrants and lower two quadrants of the segmented photodiode. The feedback loop maintains a constant deflection (thus a constant force) between the tip and the sample by adjusting the z-height of the tip above the sample. By recording the zheight changes with the x-y position, one can obtain information about the topography of the sample.

3.3 Piezoresponse Force Microscopy

Piezoresponse force microscopy measures the mechanical response when an electrical voltage is applied to the sample surface with a conductive tip of an AFM. In response to the electrical stimulus, the sample then locally expands or contracts as shown in Figure 3.3.

When the tip is in contact with the sample and the local piezoelectric response

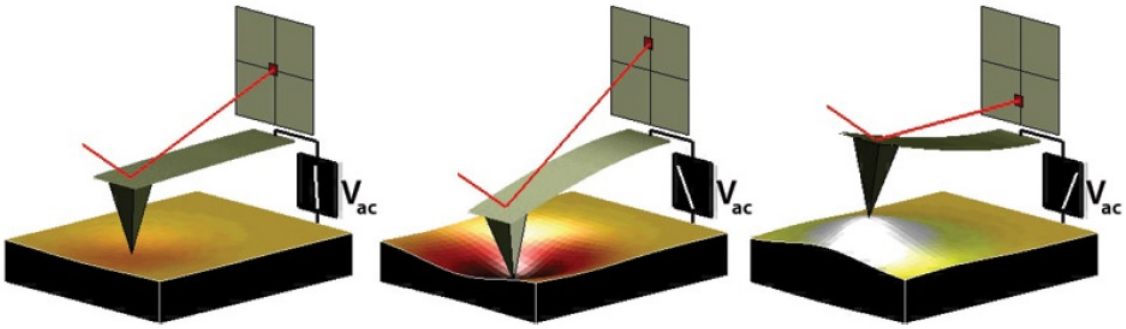

Figure 3.3: Depiction of PFM operation. The sample deforms in response to the applied voltage. This, in turn, causes the cantilever to deflect, which can then be measured and interpreted in terms of the piezoelectric properties of the sample [11].

is detected as the first harmonic component of the tip deflection, the phase ϕ, of the electromechanical response of the surface yields information on the polarization direction below the tip. For c^- domains (polarization vector oriented normal to the surface and pointing downward), the application of a positive tip bias results in the expansion of the sample, and surface oscillation are in phase with the tip voltage, $\phi = 0$. For c^+ domains, the response is opposite and $\phi = 180°$.

3.3.1 Piezo Effect

The relationship between the strain and the applied electric field (often referred to as "inverse piezo effect") in piezoelectric materials is described by a rank-3 tensor. The most important component of this tensor is the d_{33} component since couples directly into the vertical motion of the cantilever. The voltage applied to the tip is

$$V_{tip} = V_{dc} + V_{ac}cos(\omega t), \tag{3.2}$$

resulting in piezoelectric strain in the material that causes cantilever displacement

$$z = z_{dc} + A(\omega, V_{ac}, V_{dc})cos(\omega t + \phi) \tag{3.3}$$

due to piezoelectric effect. When this voltage is driven at a frequency well below that of the contact resonance of the cantilever, this expression becomes

$$z = d_{33}V_{dc} + d_{33}V_{ac}cos(\omega t + \phi) \tag{3.4}$$

where d_{33} is implicitly assumed to be dependent on the polarization state of the material. From this last equation and from Figure 3.4, the magnitude of the oscillating response is a measure of the magnitude of d_{33} and the phase is sensitive to the

polarization direction of the sample. Typical values for d_{33} range from 0.1pm/V for weak piezo materials to 500pm/V for the strongest.

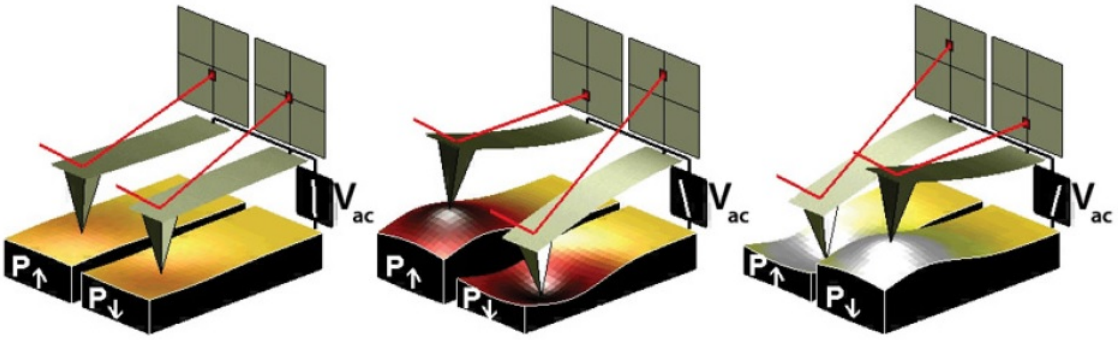

Figure 3.4: Sign dependence of the sample strain. When the domains have a vertical polarization that is pointed downwards/upwards and a positive voltage is applied to the tip, the sample will locally expand/contract. The phase of the measured response is thus proportional to the direction of the domain polarization [11].

The direction of the sample polarization determines the sign of the response as shown in Figure 3.4. If the polarization is parallel and aligned with the applied electric field, the piezo effect will be positive, and the sample will locally expand. If the local sample polarization is anti-parallel with the applied electric field, the sample will shrink locally. This sign-dependent behavior means that the phase of the cantilever provides an indication of the polarization orientation of the sample when an oscillating voltage is applied to the sample.

Chapter 4

Experiments

4.1 Yttrium Nickel Manganese Oxide

Yttrium nickel manganese oxide (YNMO), a compound having a double perovskite structure was theoretically proposed to be a multiferroic in 2010 [1]. It was synthesized by some groups recently and few properties about this material are known [13][14]. Till now it has not been confirmed as a multiferroic at any temperature. The bulk

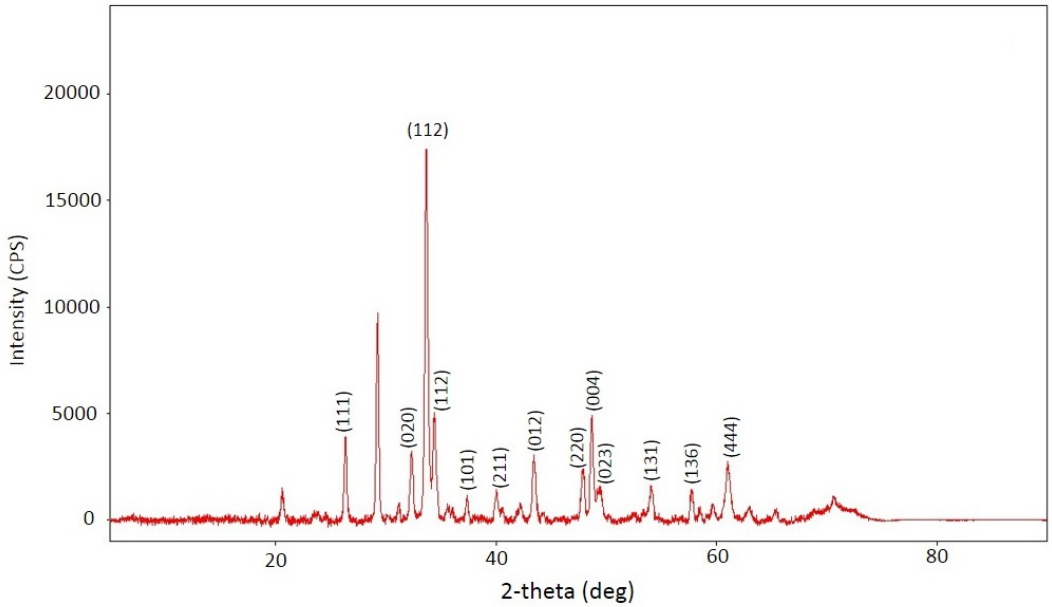

Figure 4.1: X-ray diffraction peaks of YNMO which matches the data produced by Tang et.al. [13]

material was prepared using the conventional solid state reaction approach using yttrium oxide (Y_2O_3), nickel oxide (NiO) and manganese dioxide (MnO_2) as the raw materials. Reactants were thoroughly mixed in an ethanol environment to create a homogeneous mixture. A pellet was made of the mixture and heated in the furnace

at $1000°C$ for 24 hours for sintering. This process mainly involves atomic diffusion for the formation of the product from its reactants. The X-Ray diffraction peaks of the bulk material are shown in Figure 4.1

The YNMO thin film was deposited on strontium titanium oxide (STO) substrate. The STO $\langle 110 \rangle$ was first annealed in an oxygen environment at 5×10^{-1} mbar pressure for 12 hours. The film was deposited using pulsed laser deposition technique. The KrF excimer laser was operated at 2 Hz frequency and 6000 shots were fired on the target. The temperature of the substrate was maintained at $800°C$.

The YNMO thin film on STO substrate was analyzed using atomic force microscopy. The topography of the film is shown in Figure 4.2.

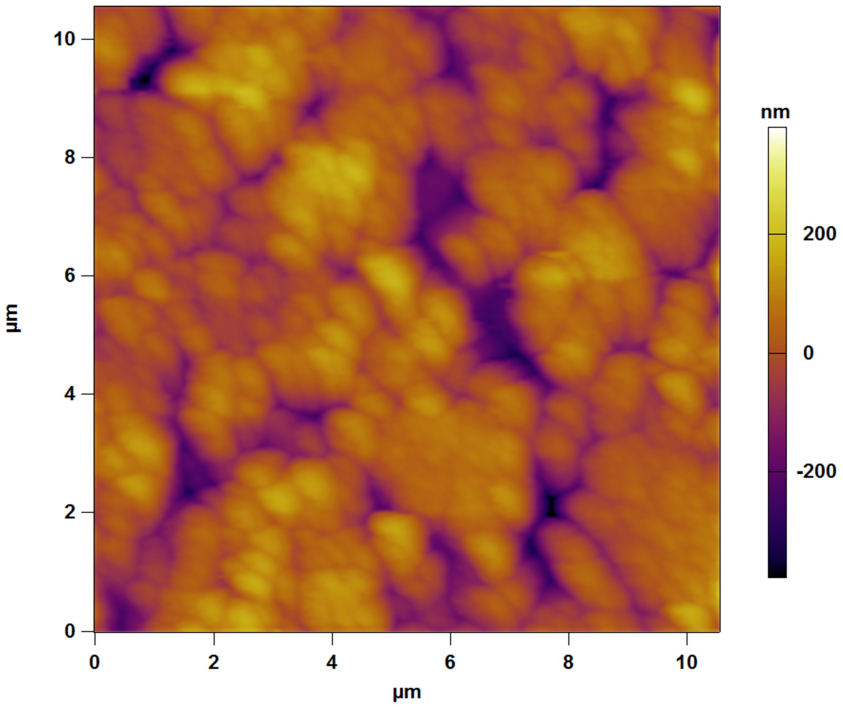

Figure 4.2: AFM image showing topography of YNMO thin film on STO $\langle 110 \rangle$ substrate. The imaging was done in contact mode.

To see signs of ferroelectricity in the material, piezoresponse force microscopy was used on both bulk sample and the thin film. Both bulk and thin film show hysteresis as shown in Figure 4.3

Some domain-like structures were also seen on bulk YNMO sample while looking at the topography of the material in contact mode as shown in Figure 4.4

Unfortunately, piezoresponse force microscopy alone cannot confirm the ferroelectricity in a material. On our system it was seen that the response may also come from the surface on which the sample is being investigated. For example, in this case the response shown by the thin film of YNMO on STO $\langle 110 \rangle$ substrate is probably because of the substrate itself. Later it was confirmed that STO $\langle 110 \rangle$ itself is a

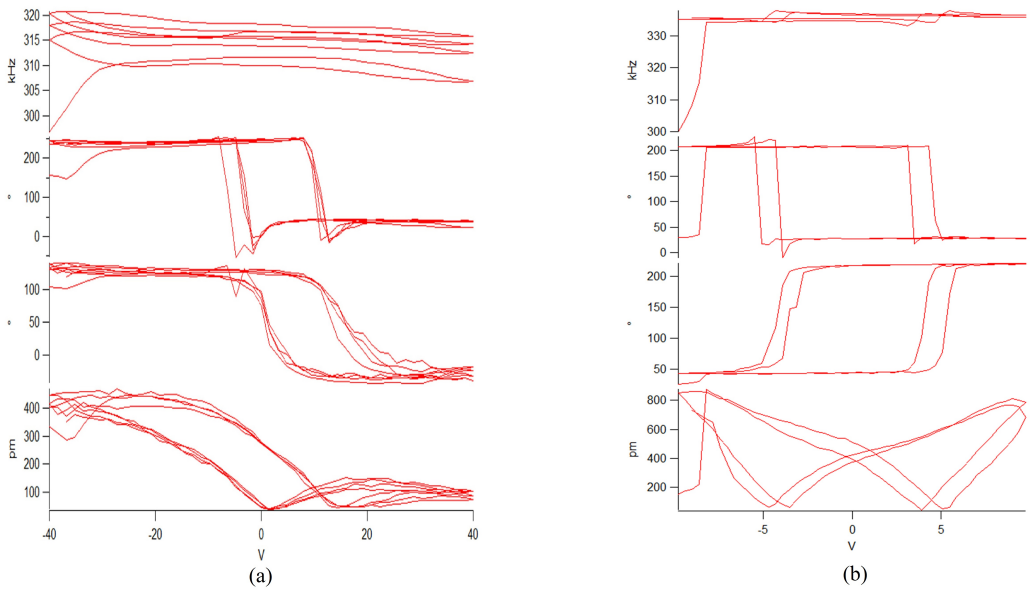

Figure 4.3: (a) Ferroelectric hysteresis loop and piezoelectric butterfly loop in bulk YNMO; (b) Ferroelectric hysteresis and piezoelectric loops in YNMO thin film on STO ⟨110⟩ substrate.

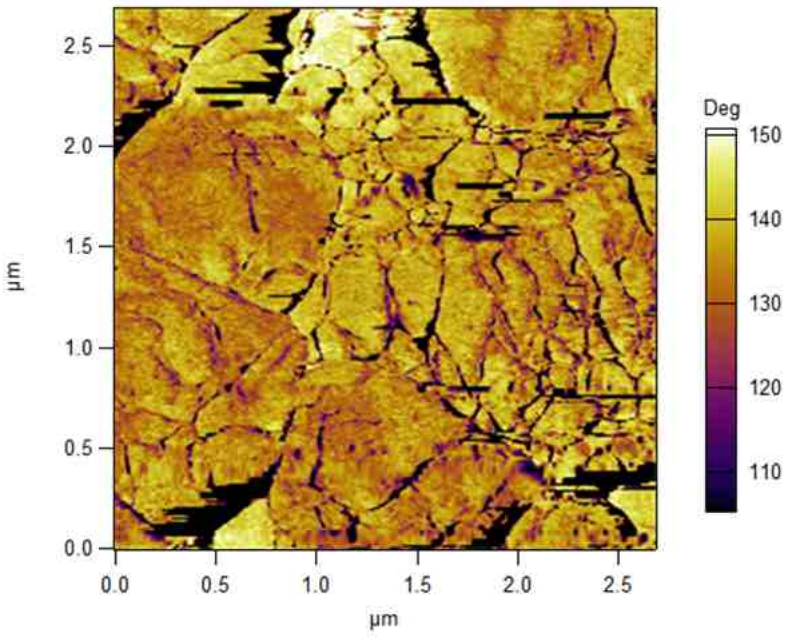

Figure 4.4: Domain-like structures seen on bulk YNMO.

ferroelectric at room temperature which was previously unknown. Figure 4.5 shows the ferroelectric and piezoelectric hysteresis of STO ⟨110⟩.

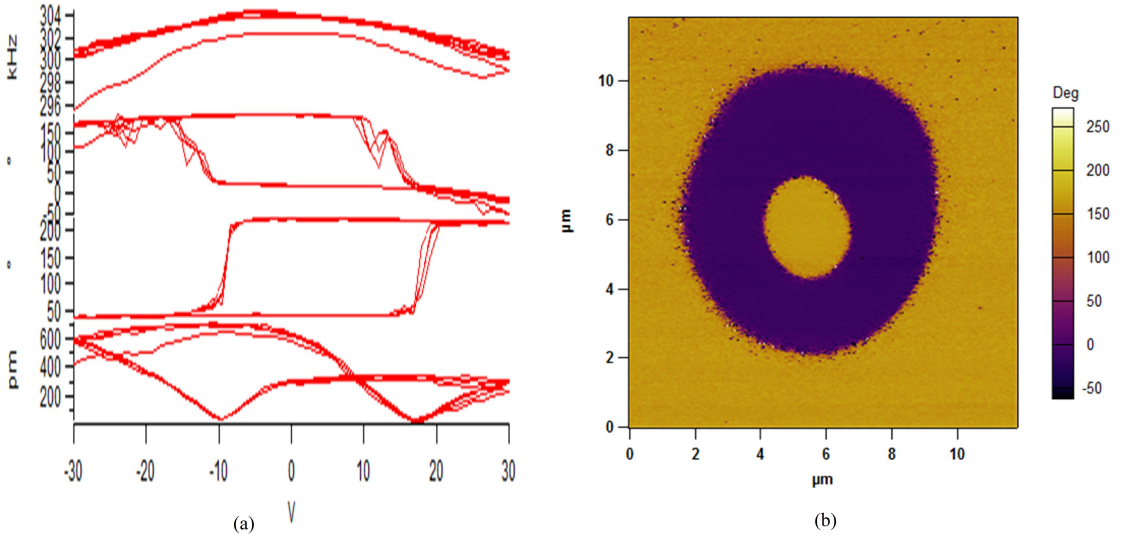

Figure 4.5: (a) Ferroelectric and piezoelectric hysteresis curves of STO substrate at room temperature; (b) PFM lithography done on STO substrate.

4.2 Lanthanum Strontium Manganese Oxide

Lanthanum strontium manganese oxide, a perovskite structure material, was prepared using the reactants lanthanum oxide (La_2O_3), strontium carbonate ($SrCO_3$) and manganese dioxide (MnO_2). The stoichiometric ratio was kept such that the strontium doping level was one third, $x = 0.33$. For this value of doping, LSMO behaves like a *half-metal*. The reactants were mixed using ethanol forming a homogeneous mixture. A pellet was formed, but it absorbed moisture when kept overnight. This was due to lanthanum oxide which absorbs moisture to form lanthanum hydroxide.

$$La_2O_3 + 3H_2O \longrightarrow 2La(OH)_3 \tag{4.1}$$

The pellet was crushed and the powder was heated to remove moisture. A pellet was formed again, put into a silica crucible and kept in a furnace at $1450°C$ for sintering for 24 hours. The X-ray diffraction analysis ,as shown in Figure 4.6, shows that the desired crystalline material was not formed; instead an amorphous mixture was formed.

However, since the stoichiometry did not change, the material obtained was used as a target to make thin films of LSMO using pulsed laser deposition. The substrate used was LSAT $\langle 100 \rangle$ which was first annealed at 1 mbar pressure of oxygen for 12 hours. Pulsed laser deposition of the LSMO target was done using a KrF excimer laser, 10000 shots at 2 Hz. The thin film obtained was granular as shown in Figure 4.7

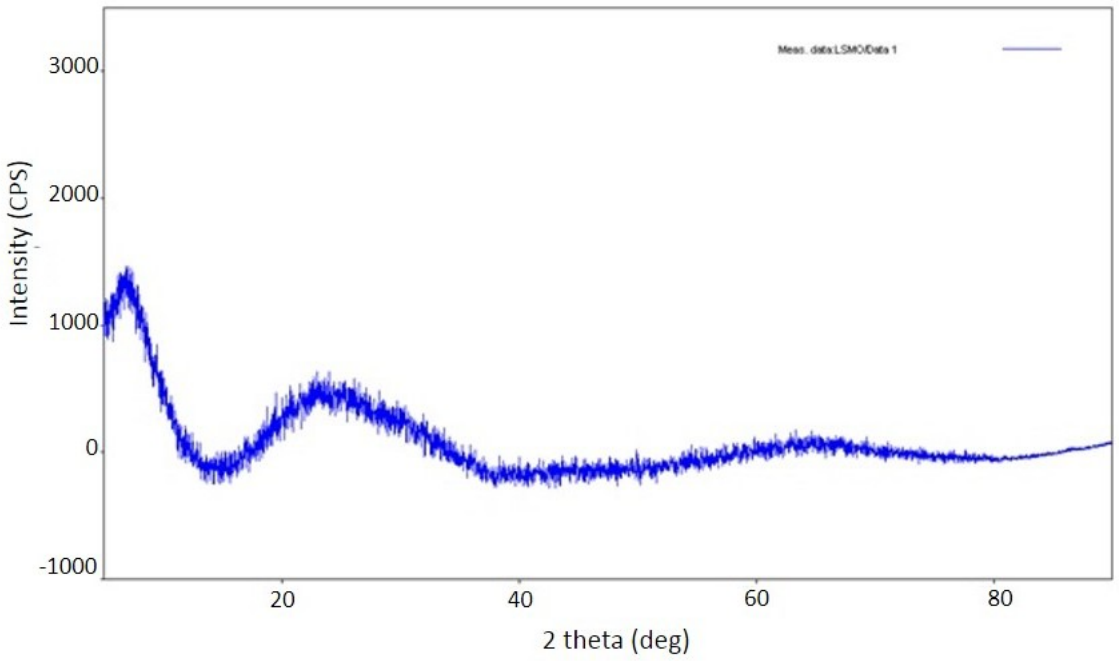

Figure 4.6: Amorphous like X-ray diffraction of bulk LSMO showing that crystal structure was not formed.

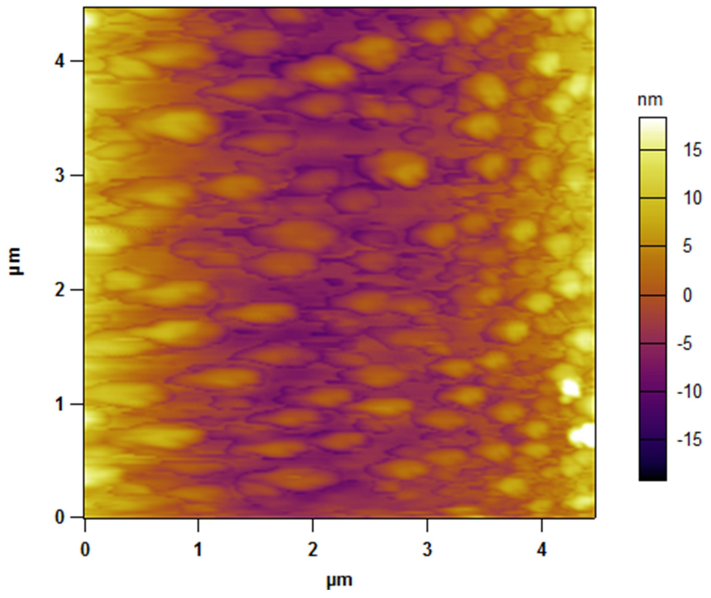

Figure 4.7: A granular thin film of LSMO grown on LSAT $\langle 100 \rangle$ substrate

4.3 Future Prospects

YNMO has shown some signs of ferroelectricity, as seen in the previous section, but it hasn't been confirmed as a ferroelectric at room temperature. PFM measurements in a varying external magnetic field will confirm whether polarization in YNMO can be changed by magnetic fields. Probing electric and magnetic properties at lower

temperatures may yield interesting results.

LSMO is a known room temperature ferromagnet, and it has been confirmed that STO $\langle 110 \rangle$ is a room temperature ferroelectric. Both LSMO and STO have a perovskite structure. An epitaxial thin film of LSMO on STO substrate could be a very interesting material as the interface of the two materials may act as a composite multiferroic system.

Bibliography

[1] Sanjeev Kumar et al., Theoretical prediction of multiferroicity in double perovskite Y_2NiMnO_6, Phys Rev B 82, 134429 (2010)

[2] Tuomas Lahtinen, Ferromagnetic-Ferroelectric Domain Coupling in Multiferroic Heterostructures, Department of Applied Physics, Aalto University publication series Doctoral Dissertations (2013)

[3] Dragan Damjanovic, The Science of Hysteresis volume 3, Elsevier (2005)

[4] Hans-Ulrich Krebs et al., Pulsed Laser Deposition (PLD) - a Versatile Thin Film Technique,

[5] A. R. Cunliffe, Magnetoelectric cobalt ferrite/bismuth ferrite hybrid nanostructures: Progress towards achieving electric field control of magnetization, Senior Honors Thesis, Northwestern University, Illinois (2009)

[6] Ruth Mckinnon, Studies of new multiferroics, Masters Thesis, University of Warwick (2011)

[7] S. W. Cheong and M. Mostovoy, Multiferroics : A magnetic twist for multiferroicity, Nature Materials volume 6 (2007)

[8] A. Yourdkhani, Synthesis and Characterization of Ferroic and Multiferroic Nanostructures by Liquid Phase Deposition, University of Orleans Theses and Dissertations, paper 1579 (2012)

[9] Du, Yi, Multiferroic transition metal oxides: structural, magnetic, ferroelectric and thermal properties, PhD Thesis, University of Wollongong, Institute for Superconducting and Electronic Materials (2011).

[10] Asylum Research, Atomic Force Microscopes, MFP-3D Manual, Version 04-08 (2008)

[11] Asylum Research, Piezoresponse force microscopy, Manual (2013)

[12] Nandang Mufti, Introduction to Multiferroic Materials; Classifications and Mechanisms, Department of Physics, Universitas Negeri Malang (2009)

[13] M. H. Tang et al., The giant dielectric tunability effect in bulk Y_2NiMnO_6 around room temperature, Appl Phys A 105:679-683 (2011)

[14] T. Siritanon et al., Synthesis, characterization and dielectric properties of Y_2NiMnO_6 ceramics prepared by a simple thermal decomposition route, J Mater Sci: Mater Electron 25: 1361-1368 (2014)

[15] T Kimura, Spiral Magnets as Magnetoelectrics, Annu. rev. mater. Res. 37, 387-413 (2007)

[16] Y Du et al., Magnetic properties of Bi_2FeMnO_6: A multiferroic material with double perovskite structure, Appl. Phys. Lett. 97, 122502 (2010)

[17] M. Kitamura, Ferromagnetic properties of epitaxial La_2NiMnO_6, Appl. Phys. Lett. 94, 132506 (2009)

[18] Y Zhang et al, Demonstration of magnetoelectric read head of multiferroic heterostructures, Appl. Phys. Lett. 92, 152510 (2008)

[19] L.W. Martin et al., Multiferroics and magnetoelectrics: thin films and nanostructures, J. Phys.: Condens. Matter 20, 434220 (2008)

[20] Sergei V. Kalinin and Dawn A. Bonnell, Imaging mechanism of piezoresponse force microscopy of ferroelectric surfaces, Physical Review B, Volume 65, 125408 (2002)